Acta Materialia 273 (2024) 119954

Contents lists available at ScienceDirect

Acta Materialia

journal homepage: www.elsevier.com/locate/actamat

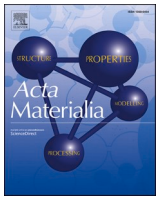

Full length article

Effects of structural hierarchy and size on mechanical behavior of nanoporous gold

Hansol Jeon [a,b], Jürgen Markmann [a,c,*], Shan Shi [d,a]

[a] Institute of Hydrogen Technology, Helmholtz-Zentrum Hereon, 21502 Geesthacht, Germany
[b] Department of Advanced Materials Engineering, Keimyung University, Daegu 42601, Republic of Korea
[c] Institute of Materials Physics and Technology, Hamburg University of Technology, 21073 Hamburg, Germany
[d] Research Group of Integrated Metallic Nanomaterials Systems, Hamburg University of Technology, 21073 Hamburg, Germany

ARTICLE INFO

Keywords:
Nanoporous gold
Hierarchical structure
Compressive test
Size effect
Electrochemically tunable strength
Microcompression

ABSTRACT

Nanoporous gold with a hierarchical structure has prospects as an advanced functional material with enhanced mechanical properties, but how the hierarchical structure affects its mechanical properties compared to a unimodal structure has not been revealed. Here, we investigate the mechanical behavior of hierarchically-structured nanoporous gold and unimodally-structured nanoporous gold with the same relative density by micropillar compressive tests in dry and electrolyte environment. The ligament size at the upper-level structure in hierarchically-structured nanoporous gold and the ligament size in unimodally-structured nanoporous gold are kept similar, while having hierarchically-structured samples with ligament sizes of 10 to 50 nm at lower-level structure. We find that hierarchically-structured nanoporous gold shows greater compressive strength and pronounced stress-variation by oxidization of the surface compared to unimodally-structured nanoporous gold. A ligament-size dependency on the lower-level structure in hierarchical samples is observed, with compressive strength and stress variation by surface oxidation increasing as the lower-level ligament size decreases. Three-dimensionally reconstructed structure analysis suggests that the enhanced mechanical properties of hierarchically-structured nanoporous gold are attributed to the better-connected network of ligaments originating from two separated dealloying-coarsening procedures. The influence of dislocation activities depending on characteristic sizes is also discussed to elucidate the distinguished mechanical behavior.

1. Introduction

Nanoporous gold (NPG), a bi-continuous structure composed of nanoscale ligaments and pores, has both merits of physical and chemical properties coming from a nanostructure of the noble metal Au [1–3]. NPG has served as a model material for studying the small-scale mechanics of nanoporous metals or random nanoscale metal networks in general. Their mechanical properties are important for their application as lightweight high-strength structural materials or functional materials such as actuation materials, strain-sensing materials, and responsive materials with switchable mechanical behavior [4–5]. Thus, studies to improve its mechanical properties have been conducted in various approaches—controlling the ligament size, relative density, and microstructure as key parameters affecting the mechanical behavior [6–14]. Meanwhile, hierarchical nanoporous gold (HNPG)—as a novel strategy to enhance its properties—has been recently established [15], which features multiple levels of open-cell structure with nanoscale ligaments and pores in a material. By transforming the existing solid ligament structure into an additional open-cell structure, HNPG can be lighter due to lower relative density and more sensitive to electrochemical reactions due to higher surface area as compared to NPG [15,16].

For the fabrication of a hierarchical structure, so far the atomic fraction of Au has to be kept below 15% in order to enforce a two-step dealloying processes [15–20], which inevitably results in a very low relative density, when compared to typical NPG with an Au atomic fraction ranging from 15% to 42% [3,9,10,12,21]. This inherent gap in the relative density between HNPG and NPG makes a comparison of their mechanical properties challenging. The fabrication of NPG and HNPG from Au of 15 at.% have been separately reported [20,21], and Shi *et al.* [15] anticipated that HNPG would exhibit the better mechanical properties compared to NPG based on the proposed scaling law. However, a direct comparison between the mechanical behavior of

* Corresponding author.
E-mail address: j.markmann@tuhh.de (J. Markmann).

https://doi.org/10.1016/j.actamat.2024.119954
Received 4 March 2024; Received in revised form 19 April 2024; Accepted 21 April 2024
Available online 25 April 2024

HNPG and NPG with the same relative density for both in order to investigate how the hierarchical structure influences the mechanical behavior of nanoporous gold is still missing.

The size of the ligaments has been an effective factor in tuning the mechanical properties of nanoporous gold, with the ligament-size dependent mechanical behavior, in line with a trend of size-effect at the nanoscale [22–25]. Its widely tunable size, ranging from nanometer to micrometer scale, provides opportunities to explore fundamental research based on its mechanical behavior related to dislocation activities [7-10,26-28]. In HNPG, the size-effect on its mechanical behavior has not yet been revealed, but it will be more tangled owing to the multiple structural levels of different sizes within a single open-cell structure. This indicates that there is a need to understand whether and how the ligament size in HNPG affects the mechanical properties. Moreover, since it is a rather recent material, the investigation of mechanical properties has not been systematically carried out so far.

The mechanical tests in electrochemical environment allow the surface state of nanoporous gold to be controlled *in-situ* during mechanical testing [4,5,27,29-33]. By imposing a corresponding electrode potential up to the OH adsorption regime, a monolayer oxide is covered on the ligament surface; reversely, the covered monolayer oxide can be reduced by switching the potential to the desorption regime. This surface state change can affect the dislocation activities especially at or close to the surface, leading to a tunable mechanical behavior. It has been revealed that the yield strength and flow stress can enhance when the surface of ligaments was covered with a monolayer oxide, and the enhancement was found to be highly related to the microstructure such as ligament size [30,31]. Moreover, by in-situ compressive tests of coarse-grained and nanocrystalline NPG in an electrochemical environment, Zheng *et al.* [27] decoupled the effect of surface triple junctions from grain boundary and surface effect on the strength of nanoporous gold. Hence, the mechanical tests in electrochemical environment can provide a better understanding of the mechanical behavior—particularly the governing mechanism for plasticity—in nanoporous gold. In addition, the mechanical tests of HNPG in electrochemical environment have not been studied yet, so, it would be fascinating to investigate the effect of oxidized state induced by applied potential for HNPG, especially in comparison to the response of NPG.

Here, we report the mechanical behavior of HNPG and NPG with the same relative density by performing micropillar compression in an electrochemical environment. Three HNPG and one NPG sample were prepared from the same $Ag_{85}Au_{15}$ precursor alloy, with similar ligament sizes in the upper-level structure of HNPG and in NPG, and with different ligament sizes ranging from 10 nm to 50 nm in the lower-level structure in HNPG. Our findings reveal a higher compressive strength and greater flow stress variation by the reversible surface oxidation/reduction of HNPG than that of NPG. In addition, we find that both the strength and stress variation of HNPG exhibit a strong ligament-size dependence at the lower-level structure.

2. Experimental methods

2.1. Sample preparation

Three HNPG and one NPG samples were prepared from the same $Ag_{85}Au_{15}$ precursor alloy. It is noteworthy that the precursor alloy of $Ag_{85}Au_{15}$ was adopted in this study, unlike Shi *et al.* [15] and Riedel *et al.* [17], who used $Ag_{93}Au_7$ and $Ag_{90}Au_{10}$ as the precursor alloy, respectively. These low gold contents would not allow for the fabrication of unimodal NPG of comparable density to the corresponding HNPG what is one of the key strategies in this study. HNPG samples with different lower-level ligament size L_1 but similar upper-level ligament size L_2 were fabricated via a dealloying-coarsening-dealloying strategy by refining the protocol by Shi et al. [15]. The NPG sample was prepared by coarsening the as-prepared HNPG sample, having a ligament size L similar to the upper-level ligament size L_2 of HNPG. It is important to note that this approach is to derive a low volume shrinkage during dealloying and post-annealing process from the precursor alloy of $Ag_{85}Au_{15}$, and prepare NPG with a relative density similar to HNPG samples (further discussed in Section 3.1.).

The precursor alloy of $Ag_{85}Au_{15}$ was fabricated by melting pure Ag (99.99%, WIELAND Edelmetalle) and Au (99.99%, Sindlhauser Materials) wires in an arc melter (MAM-1, Edmund Bühler) under an argon atmosphere, followed by a homogenization at 850°C for 5 days in a vacuum. The precursor alloy was cold-rolled to a plate shape and cut into cuboid-shape pieces with the dimension of $0.8 \times 0.8 \times 0.2\ mm^3$ by a diamond wire saw (model 3032–4, Well Diamond Wire Saws). These pieces were polished up to 0.25 μm diamond suspension. Thermal annealing was conducted at 600°C for 4 h in a vacuum furnace (MILA-5000, ULVAC) in order to relieve stress induced by cutting and polishing processes.

A two-step dealloying-process was carried out to fabricate HNPG samples as shown in Fig. 1. During the first dealloying step, a nanoporous $Ag_{70}Au_{30}$ alloy was prepared by partially dissolving the Ag component of the precursor alloy through electrochemical dealloying in 0.01 M H_2SO_4 aqueous solution prepared out of 96% (Supelco, Merck) and ultrapure water (Arium Comfort I TOC, Sartorius) with an AgCl coated Ag wire and a pure Ag wire as a reference electrode (RE) and counter electrode (CE), respectively. The pseudo Ag/AgCl reference electrodes were calibrated versus a standard hydrogen electrode (SHE, HydroFlex, Gaskatel) in the same electrolyte that was used for the dealloying, which showed +0.622 (±0.003) V in 0.01 M H_2SO_4 and +0.515 (±0.003) V in 1.0 M $HClO_4$ aqueous solution. Hereafter, all electrode potentials used in this paper are presented relative to SHE. A constant electrode potential of 1.073 V was imposed for the first dealloying step until the charge density reached 400 C/g. Afterwards, the dealloyed nanoporous alloy with a residual Ag content ($Ag_{70}Au_{30}$) was coarsened at 550°C for 1 hour in vacuum (MILA-5000, ULVAC), which established the size of the upper-level structure. At the second dealloying, the hierarchical nanoporous structure was formed by dissolving the remaining Ag component in the coarsened nanoporous $Ag_{70}Au_{30}$ alloy, simultaneously inserting the additional nanoporous structure (lower-level structure) into the existing alloy ligaments. The second dealloying was conducted in 1.0 M $HClO_4$ aqueous solution, diluted from 60% $HClO_4$ (Supelco, Merck) and ultrapure water, with a constant electrode potential of 1.340 V and 1.515 V for 2 h each, followed by five potential cycles from 0.855 V to 1.515 V at a scan rate of 5 mV/s with replacing the Ag wire by porous carbon cloth as CE. All dealloying processes were conducted in three-electrode electrochemical cells with the potential control through a potentiostat (Autolab PGSTAT302N, Metrohm). The lower-level ligament size L_1 was adjusted by a post thermal treatment on the as-prepared HNPG at 200°C and 250°C, respectively, for 30 min in vacuum (MILA-5000, ULVAC). NPG was fabricated by annealing the as-prepared HNPG at 600°C for 1 hour in argon environment (infrared furnace behr IRF 10, behr Labor-Technik) through rearranging and agglomerating the hierarchical structure to a unimodal structure.

2.2. Structural characterization

Chemical composition of the nanoporous alloy after first dealloying and residual Ag in the as-prepared HNPG were measured by an energy-dispersive X-ray spectroscopy unit (EDS) installed in a dual-beam FIB (focused ion beam) and SEM (scanning electron microscope) system (Helios G4 PFIB UXe, ThermoFisher) at several locations from edge to center. Relative density of HNPG and NPG samples was determined by measurement of the weight and volume relative to the density of Au, 19.3 g/cm^3. Three ligament sizes, L_1 and L_2 for HNPG, and L for NPG, were determined by measuring the diameter of ligament's neck in connected ligaments, possibly the thinnest parts, from SEM pictures. At least 50 ligaments were measured at different positions in the SEM for each sample.

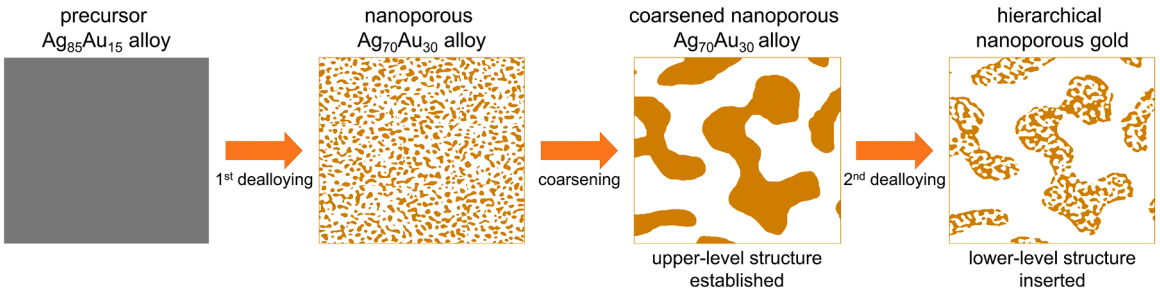

Fig. 1. Schematic of the fabrication procedure for HNPG by a two-step dealloying process: first dealloying of precursor $Ag_{85}Au_{15}$ alloy, followed by coarsening of nanoporous $Ag_{70}Au_{30}$ alloy to establish the upper-level structure, and second dealloying on coarsened nanoporous $Ag_{70}Au_{30}$ alloy to insert additional ligament-pore structure (lower-level structure) into existing alloy ligament structure by dissolving remaining Ag component.

2.3. Mechanical testing

Micropillars of HNPG and NPG with a diameter of 8 μm and a height-diameter aspect ratio of 2 were prepared by Ga^+ FIB milling in a dual-beam FIB/SEM (Nova 200 nanolab, ThermoFisher). Compressive tests on micropillars were performed in a nanoindenter (Hysitron TI980 tri-boindenter, Bruker) with an electrically insulated flat-punch sapphire tip.

The *in-situ* setup for the compressive tests is shown in Fig. 2(a), where HNPG or NPG samples served as the working electrode (WE). A platinum wire and a commercial Ag/AgCl/3 M KCl electrode (Driref-2, World Precision Instruments) were used as the CE and RE, respectively, and 0.5 M NaF was used as the electrolyte. This is because the comprised F^- ions are non-specifically adsorbed on the gold surface [29] and 0.5 M NaF is a weak base which minimizes the damage to the nanoindenter when considering that the distance between the equipment and electrolyte are very close during the running of compressive tests [33]. The potential of the commercial Ag/AgCl electrode was checked to be 0.210 V vs. SHE in the same electrolyte. As presented in Fig. 2(b), the electrochemical behavior was measured by cyclic voltammetry at a constant scan rate of 5 mV/s in the electrolyte before the compressive tests. The curve of the cyclic voltammogram shows an adsorption peak at positive potential and desorption peak at negative potential, indicating the reversible adsorption and desorption of an OH monolayer on the ligament Au surface depending on the applied potential. Two potential values were used for compressive tests: −0.2 V corresponding the clean surface (CS) and 1.4 V corresponding to the OH covered surface, i.e., monolayer oxidized surface (OS). The compressive tests were performed under three constant environmental conditions: dry (without electrolyte), −0.2 V (CS), and 1.4 V (OS). The experiments with potential jumps, i.e., switching the potential between −0.2 V (CS) and 1.4 V (OS), during the compression were also carried out in the electrolyte environment. All tests were performed at a constant strain rate of 0.001 s^{-1}.

2.4. 3D reconstruction

3D reconstructions for HNPG and NPG samples were conducted in a dual-beam FIB/SEM system (Helios G4 PFIB UXe, ThermoFisher). All porous structures were infiltrated with epoxy (EpoThin 2, Buehler) to obtain clear 2D slice images. Trenches were milled out on the left, right, and bottom of the area of interest (AOI), and platinum was deposited on the top of the AOI as a protective layer. Serial cross-sectioning and taking SEM images were automatically carried out by an auto slice and view program with the conditions of 30 kV accelerating voltage with 0.1 nA Xe^+ plasma beam current for cross-sectioning and 5 kV voltage and 0.2 nA beam current using a through-the-lens detector (TLD) for obtaining images. 15 or 20 nm of slice thickness was used for sequential sectioning. 2D slice images were reconstructed to 3D structure by Avizo software (Avizo 3D, ThermoFisher) after alignment correction, de-nosing filtering, and segmentation. Solid fraction, specific surface area, and connectivity of the skeletonized structure were calculated by the BoneJ plug-in of the ImageJ software [34,35]. At least five 3D reconstructions were performed for each sample at arbitrary positions.

3. Results

3.1. Characterization of HNPG and NPG samples

After the first dealloying, the nanoporous Ag-Au alloy has a chemical composition of around $Ag_{70}Au_{30}$. Slightly different residual Ag contents were found at the edge and the center of the cross-section of the nanoporous Ag-Au alloy after the first dealloying: the average residual Ag was 67.4 (±2.6) at.% near the edge to a depth of around 50 μm (outer region), while it was 73.2 (±2.5) at.% at the inner regions. After the second dealloying, the residual Ag in the as-prepared HNPG was 3.5 (±0.9) at.%. The composition during post thermal annealing processes was not changed. Therefore, all HNPG and NPG samples in this study have a low residual Ag content of 3.5 (±0.9) at.%.

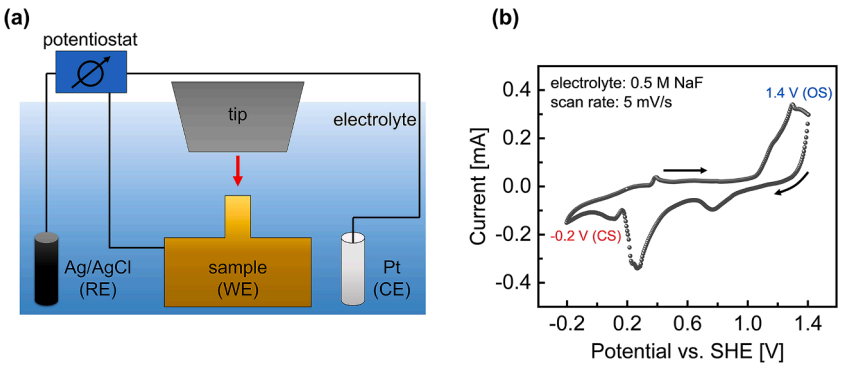

Fig. 2. (a) Schematic diagram of the *in-situ* setup for micropillar compressive tests in electrolyte under electrode potential control. (b) Cyclic voltammogram of HNPG with L_1=10 nm in 0.5 M NaF aqueous electrolyte at a scan rate of 5 mV/s.

The relative density was measured to be as around 20% for all HNPG and NPG samples by measuring the weight and dimension after fabrication of samples. This implies that the volume shrinkage occurred during the dealloying processes, while the post-coarsening on HNPG in order to control the lower ligament size or to turn it into a unimodal structure did not induce any obvious shrinkage. The micropillars were milled out a height of around 16 μm from the surface. The HNPG samples are estimated to have around 52% solid fraction at the upper-level structure and 38% at the lower-level structure, assuming identical shrinkage in both the upper-level and lower-level structures.

Fig. 3(a)–(h) show the SEM images of HNPG and NPG. For as-prepared HNPG, the upper-level ligament size is L_2 = 320 (±40) nm with the lower-level ligament size of L_1 = 10 (±2) nm (Fig. 3(a) and (e)). After post heat-treatment on the as-prepared HNPG at 200°C and 250°C for 30 min in vacuum, the upper-level ligament sizes L_2 became 320 (±37) nm and 320 (±40) nm, respectively, while the lower-level ligament sizes L_1 were coarsened to 28 (±4) nm and 48 (±8) nm, respectively (Fig. 3(b), (c), (f), (g)). These ligament sizes indicate that the upper-level ligament sizes of HNPG remain similar at around 320 nm but only the lower-level ligament sizes were coarsened from 10 nm to 50 nm. This is quite reasonable since the thermal coarsening of nanoporous gold is driven by surface diffusion with coarsening exponent $n \sim 4$ from a power law of $d \sim t^{1/n}$, where d is the ligament size, t is the coarsening time, and n is the coarsening exponent [36–39]. Therefore, the annealing conditions of 200°C and 250°C for 30 min in vacuum are insufficient for significantly coarsen the upper-level ligament structure of HNPG, since the upper-level structure is already established or, in other words, has already significantly coarsened after annealing the first step dealloyed nanoporous $Ag_{70}Au_{30}$ alloys at 550°C for 1 hour in vacuum. After a post heat-treatment at 600°C for 1 hour under an argon environment, instead of a coarsened HNPG, a unimodal NPG was formed by collapsing and rearranging the hierarchical structure. As shown in Fig. 3(d) and (h), the ligament size of the NPG was L = 330 (±48) nm, which is quite comparable to L_2 of the as-prepared and coarsened HNPG. Hereafter, the samples are referred to as HNPG with 10 nm, HNPG with 30 nm, HNPG with 50 nm, and NPG.

It should be emphasized that unimodal NPG with a ligament size of 330 nm and low relative density of 20% was successfully synthesized here despite the starting master alloy having a low initial Au content of x_{Au}= 15 at.%. By contrast, coarsened NPG made by annealing dealloyed unimodal NPG from a low x_{Au} master alloy usually involves a large volume shrinkage during both the dealloying and coarsening processes, leading to a relative density close to 30% [12,40,41]. As shown in Table 1, coarsening of NPG samples made from a master alloy with x_{Au}= 25 at.% results in a volume shrinkage of 16–36%. The relative density was as high as 29% even without post-annealing when x_{Au}= 20%. This indicates that our approach of making NPG by coarsening HNPG is a promising route for fabricating coarsened NPG samples with a relative density below 30%. Thereby, it could help to research the mechanical behavior and scaling equation for nanoporous gold extended to low relative density regions, which are still unexplored as shown in Fig. 9 (please also refer to Section 4.1.1.).

3.2. Mechanical behavior

All compressive tests were conducted at least five times for each sample and environmental condition. All the pillars for compression have a height of around 16 μm and a diameter of around 8 μm, as shown in Fig. 3(i)–(l). Fig. 4(a)–(d) present representative engineering stress-strain curves for HNPG with 10, 30, 50 nm and NPG under each environmental condition of dry, −0.2 V (CS), and 1.4 V (OS). The average flow stress at 10% strain was measured for each sample. In the dry condition, flow stress values at 10% strain for HNPG with 10 nm, 30 nm, 50 nm, and NPG are 37.9 (±1.0) MPa, 32.2 (±0.2) MPa, 25.3 (±0.9) MPa, and 5.7 (±0.2) MPa, respectively. At −0.2 V condition, they are 37.6 (±0.9) MPa, 32.9 (±0.7) MPa, 25.2 (±0.8) MPa, and 5.6 (±0.1)

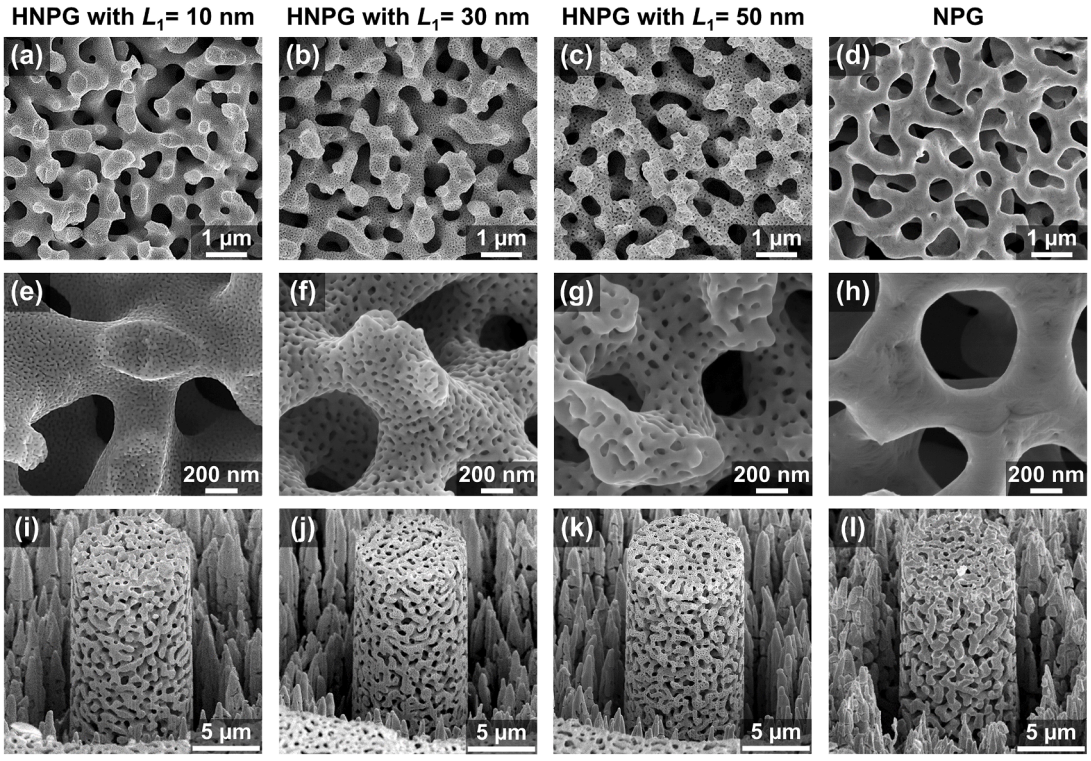

Fig. 3. SEM images for three HNPG and NPG. (a–d) Low magnification images showing similar upper-level structures for all HNPG and NPG, (e–h) high magnification images identifying different lower-level structures of HNPG and unimodal structure of NPG, and (i–l) micropillars of HNPG and NPG samples. (a,e,i): As-prepared HNPG, denoted as HNPG with 10 nm; (b,f,j): coarsened HNPG at 200°C for 30 min in vacuum, denoted as HNPG with 30 nm; (b,f,j): coarsened HNPG at 250°C for 30 min in vacuum, denoted as HNPG with 50 nm; (d,j,l): NPG obtained by annealing as-prepared HNPG at 550°C for 1 hour in Ar.

Table 1
Properties of magnitude of volume shrinkage for as-dealloyed and coarsened nanoporous gold with low relative density (< 25 %) and negligible residual Ag (< 5 at.%).

Au atomic fraction	Relative density		Volume shrinkage [%]	Residual Ag [at.%]	Ligament size [nm]	Reference
	As-dealloyed	Coarsened				
0.15		0.20	33	3.5	330	this work
0.20	0.29		45	< 1	33	Zandersons *et al.* (2021) [12]
0.25	0.26		4	< 1	32	
0.25		0.29	16	< 1	116	
0.25	0.26		4	< 2	43	Liu *et al.* (2016) [40]
0.25		0.3	20		~300	
0.25	0.266		6	3.6	19	Xie *et al.* (2021) [41]
0.25		0.34	36	3.6	~100	

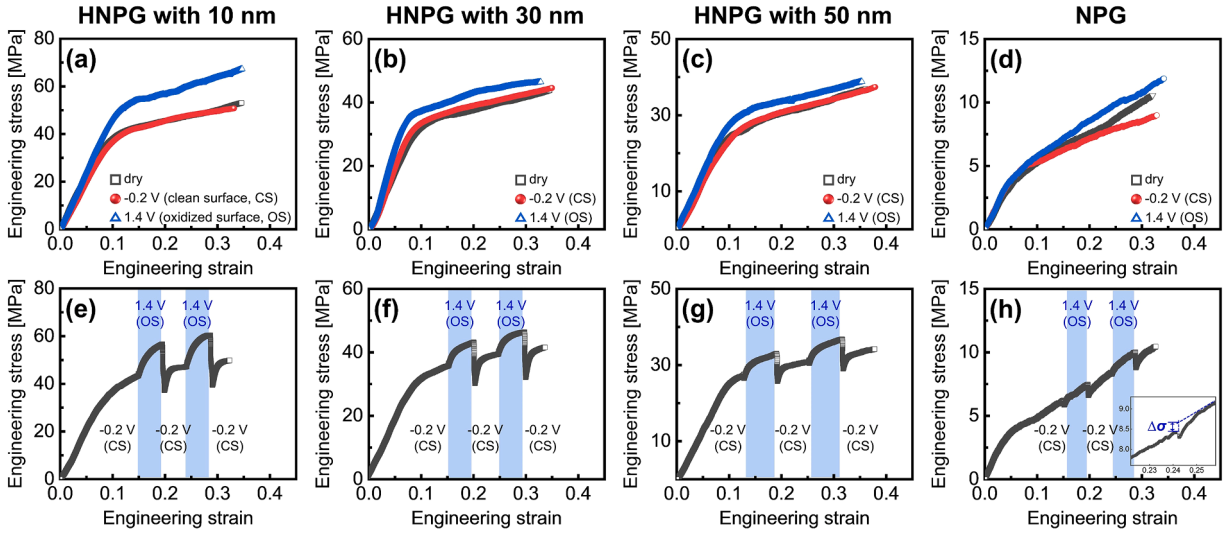

Fig. 4. Representative compressive stress-strain curves. (a–d) Compressive stress-strain curves at each constant condition of dry, −0.2 V (clean surface, CS), and 1.4 V (oxidized surface, OS). (e–h) Potential jump tests during compression, switching potential from −0.2 V (CS) to 1.4 V (OS) near strain of 15% and 25%.

MPa, while at 1.4 V, the values are 46.2 (±0.3) MPa, 37.2 (±0.2) MPa, 28.2 (±1.0) MPa, and 6.0 (±0.2) MPa, as shown in Fig. 5(a) and Table 2. This indicates that HNPG is approximately 4 to 7 times stronger than NPG, and that the strength depends on the lower-level ligament size for all three environmental conditions. The stress-strain curves in the dry state and at −0.2 V (CS) were similar, indicating negligible effects of the aqueous solution itself on the mechanical tests. In contrast, the flow stress was enhanced at 1.4 V (OS) for HNPG samples, while it seemed to be only negligibly increased for NPG.

Fig. 4(e)–(h) show representative stress-strain curves in response to potential jumps between −0.2 V and 1.4 V during the compression. The flow stress increased when the potential was switched to 1.4 V, and it returned to its initial behavior when the potential is switched back to −0.2 V, showing a reversible tunability of the flow stress by changing the surface state.

The relative variation of flow stress, $\Delta\sigma/\sigma_0 = (\sigma_{os} - \sigma_{cs})/\sigma_{cs}$, at two distinguishable surface states (CS and OS) of HNPG and NPG is plotted as a function of strain in Fig. 5(b). It shows $\Delta\sigma/\sigma_0$ is 21%±3%, 15%±2%, 11%±1%, 3% ± 1% for HNPG with 10 nm, 30 nm, 50 nm and NPG, respectively, in both 14%–15% and 23%–25% strain regimes as presented in Table 2. The stress variation by switching potential jumps on a single pillar agrees well with the enhancement of flow stress measured by applying different constant potentials on different pillars in Fig. 4(a)–(d). Both approaches confirm that surface oxidation results in the

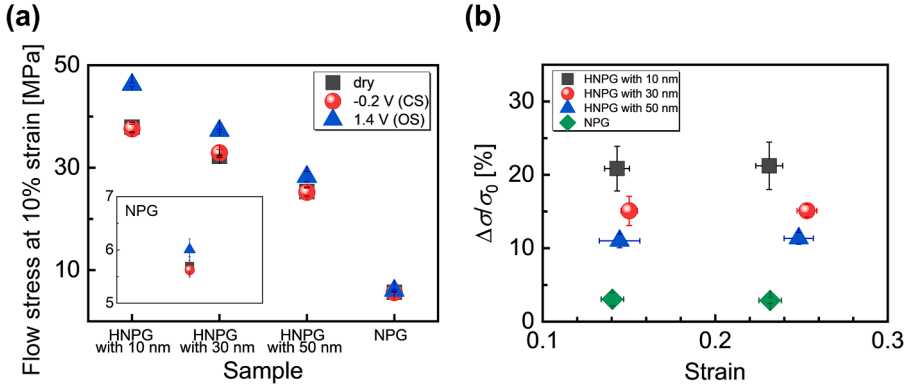

Fig. 5. (a) Flow stress at 10% strain in dry, at −0.2 V, and 1.4 V condition and (b) relative stress variation ($\Delta\sigma/\sigma_0$) at difference strains of 15% and 25% for HNPG with 10 nm, 30 nm, 50 nm, and NPG. Average values are taken from at least 5 tests of each sample, with standard deviations represented by error bars.

Table 2
Summary of comprehensive results; relative density, ligament size, flow stress at 10% strain, and stress variation for HNPG and NPG. Average values are taken from at least 5 tests of each sample, with standard deviations represented by error bars.

Sample	Relative density	Ligament size [nm]		Flow stress at 10% strain [MPa]			Stress variation ($\Delta\sigma/\sigma_0$) [%]
		Upper-level	Lower-level	Dry condition	−0.2 V condition	1.4 V condition	
HNPG with 10 nm	0.20	320 (±37)	10 (±2)	37.9 (±1.0)	37.6 (±0.9)	46.2 (±0.3)	21 (±3)
HNPG with 30 nm	0.20	320 (±37)	28 (±4)	32.2 (±0.2)	32.9 (±0.7)	37.2 (±0.2)	15 (±2)
HNPG with 50 nm	0.20	320 (±40)	48 (±8)	25.3 (±0.9)	25.2 (±0.8)	28.2 (±1.0)	11 (±1)
NPG	0.20	330 (±48)		5.7 (±0.2)	5.6 (±0.1)	6.0 (±0.2)	3 (±1)

enhancement of flow stress, but HNPG shows a much larger enhancement than NPG. It implies that the highly coarsened nanoporous gold could not exhibit the same amount of electrochemical functionality as the fine structured HNPG, which is consistent with other compression results on coarsened nanoporous gold samples [31].

Fig. 6(a)–(f) present SEM images for HNPG with 50 nm and NPG after compressive tests. For HNPG, it seems that while the upper-level structure was dominantly densified during compression, the lower-level structure almost maintained its original structure. This implies that the upper-level structure would preferentially support an external force, indicating that the plastic deformation could be mainly carried by the upper-level structure. For NPG, the structure was uniformly deformed and the typical dislocation slip bands and/or lines were observed by bending and/or shearing of the ligaments indicated by yellow arrows in Fig. 6(f).

These findings indicate the signature of the hierarchical-structure effect on the mechanical behavior because they have comparable relative density and ligament size (L_2 for HNPG and L for NPG). The findings are as follows: (1) the mechanical strength is higher in HNPG as compared to NPG, (2) the stress variation ($\Delta\sigma/\sigma_0$) is more distinct in HNPG, (3) the size-effect by lower-level ligament size for HNPG, i.e., lower-level ligament-size effect, exists in terms of flow stress and stress variation as shown in Fig. 7.

3.3. 3D reconstructed HNPG and NPG

Fig. 8(a) presents the 3D reconstructed volume for HNPG with 30 nm, 50 nm, and NPG. The reconstructed structure of HNPG with 50 nm is enlarged to show the ligaments and pores at the lower-level structure, showing that both the upper- and lower-level structures were clearly distinguished. The edge length of the reconstructed volume was set to 4 μm, corresponding to approximately 12 times of the average upper-level ligament size in HNPG (or ligament size in NPG). It is important to note that 3D reconstruction for HNPG with 10 nm was not technically feasible with keeping the representative volume due to the significant difference in size between the upper-level (L_2= ~320 nm) and lower-level structure (L_1= ~10 nm). In other words, at such low magnifications needed to maintain the representative volume for the upper-level structure, the ligaments in the lower-level structure could not be visualized. On the other hand, at higher magnifications needed to identify the lower-level ligaments, the reconstruction cannot have the representative volume. Moreover, a slicing lower than 10 nm to reconstruct ligaments in the lower-level structure has tremendous uncertainties and represents the current limit of this reconstruction method.

As presented in Fig. 8(b), the upper-level structure in the 3D reconstructed HNPG was re-embodied by filling the pores at the lower-level structure using the image filtering of the Avizo software. This step allows us to analyze the connectivity values of the upper-level and lower-level structures separately (discussed in Section 4.4.1.).

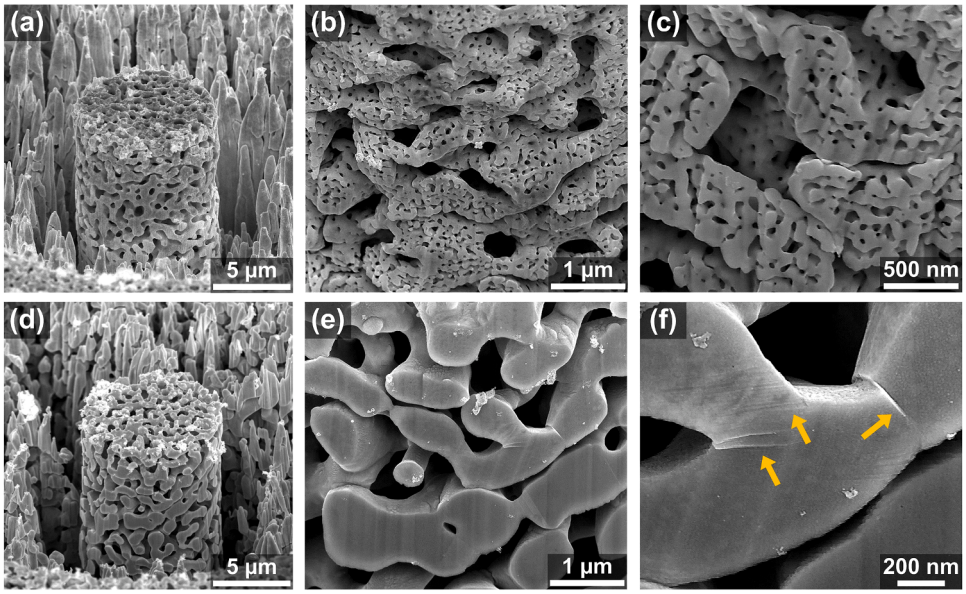

Fig. 6. SEM images after compressive tests for (a–c) HNPG with 50 nm and (d–f) NPG with slip lines marked by yellow arrows.

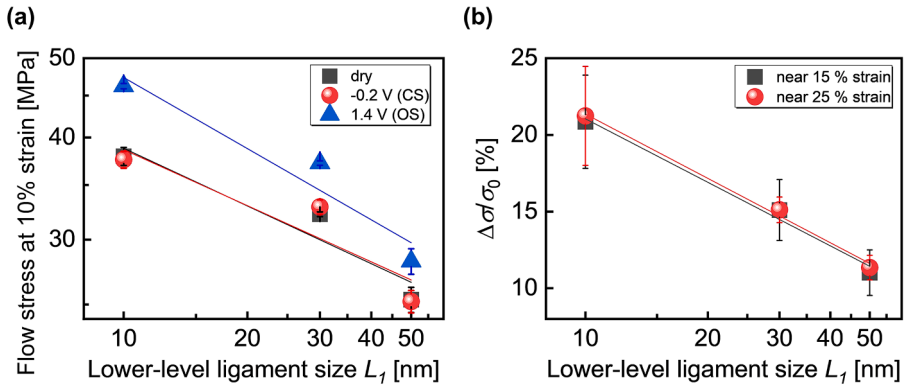

Fig. 7. Lower-level ligament-size dependent mechanical behavior. (a) Flow stress at 10% and (b) stress variation ($\Delta\sigma/\sigma_0$) as a function of ligament size at lower-level structure. Average values are taken from at least 5 tests of each sample, with standard deviations represented by error bars.

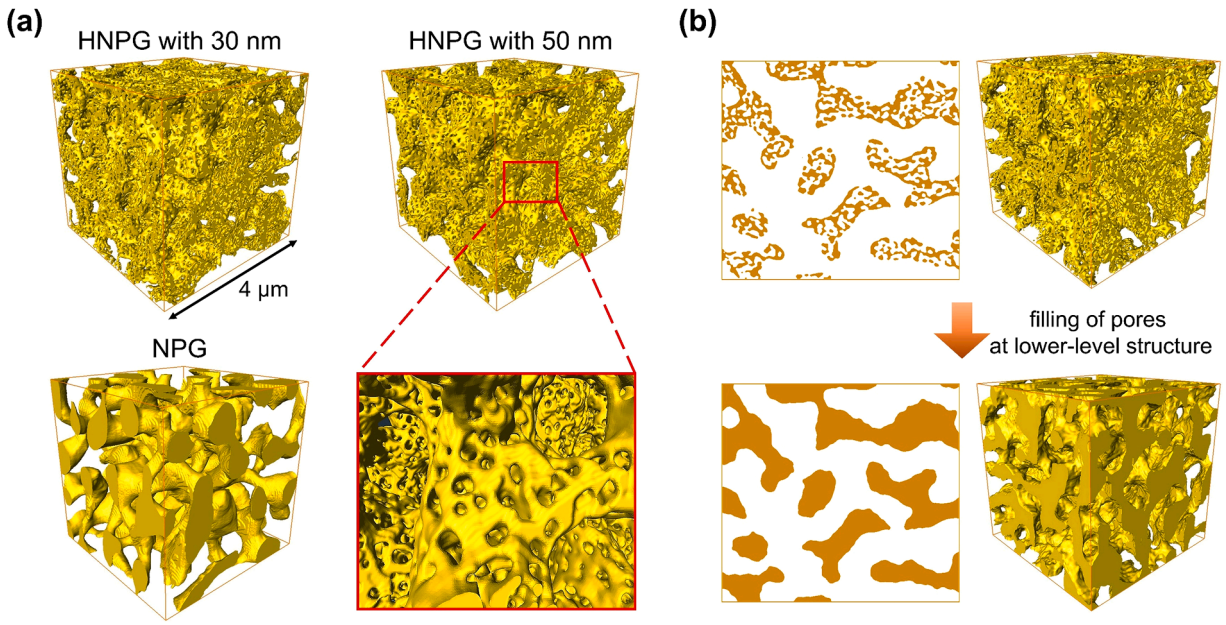

Fig. 8. (a) 3D reconstructions for HNPG with 30 nm, 50 nm, and NPG with enlarged snapshot for identifying reconstruction of lower-level structure in HNPG. (b) *Re*-embodied upper-level structure of HNPG by filling the pores at lower-level structure from the whole hierarchical structure.

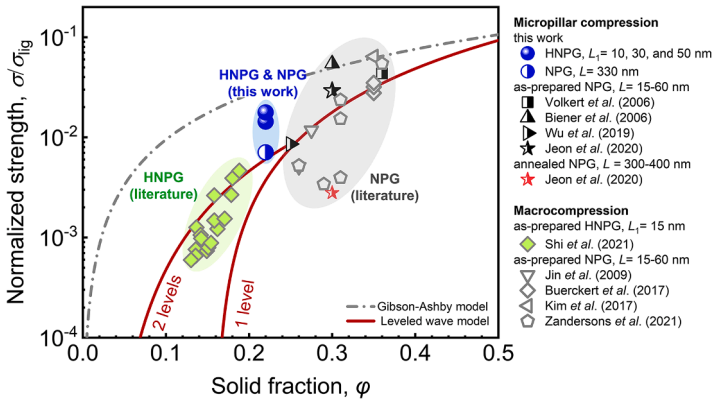

Fig. 9. Normalized strength of HNPG and NPG of this study in comparison to the results of other published studies as a function of the solid fraction: HNPG (solid symbols), NPG via micropillar compression (half-filled symbols), NPG by macrocompression (open symbols). Note that annealed sample (symbol in red) tends to extremely low strength value, probably due to the connectivity loss during the thermal coarsening as described in [51]. Micropillar compression tests, like the ones presented here, tend to slightly higher strength values than macro-compression tests.

4. Discussion

4.1. Compressive strength

The smaller the ligament size, the fewer initial dislocation sources can be accommodated and the smaller in size they are. Small dislocation sources are leading to a higher stress required to activate them stochastically [42–46]. It results in the common phenomenon of 'smaller is stronger'. HNPG has a lower-level ligament size L_1 ranging from 10 to 50 nm, so the characteristic size in HNPG is much smaller than that in NPG with L of 330 nm. Hence, the fewer dislocation sources and the limited space for them in HNPG induce a lower probability of activating dislocations and a higher stress is required to yield ligaments, which causes the higher strength in HNPG compared to NPG.

4.1.1. Scaling behavior

Fig. 9 presents normalized strength as a function of solid fraction with the scaling equation from Shi et al. [15], in addition to the experimental results of HNPG and NPG samples in this work and in literature. When only comparing the experimental results from micropillar compression (half-filled symbols) on as-prepared NPG, it seems that the normalized strengths roughly follow the equation. In the region below 25% solid fraction, there is only one set of data, namely the one studied in this work. This means that it is yet premature to describe a clear trend for predicting the strength of NPG over a wide range of relative densities. It is important to note that other references for the scaling equation could be adopted [9,10], but it is difficult to incorporate the published values into one graph, as the values of normalized strength differ due to the different approaches used to estimate the ligament strength σ_{lig} in each equation. Furthermore, when comparing the strength of NPG in this work with the coarsened NPG sample having a comparable ligament size but higher density that was obtained by annealing as-prepared NPG (named as annealed NPG, marked in red half-filled symbol in Fig. 9), it clearly shows that even though using the same micropillar compression testing method, the NPG in this work show a higher normalized strength and specific strength than the annealed NPG. This indicates that the new strategy "making coarsened NPG by annealing HNPG" in this work provides a novel route to make coarsened NPG with low density and high specific strength that typically cannot be achieved by the widely used strategy "making coarsened NPG by annealing NPG.

For HNPG, the analyzed structural data can be used to derive an expectation for the strength of the investigated samples at the different lower ligament sizes. Based on the parameters used in [15] (see Table S1 in its supporting online material), we estimate our ligament strength as 2640 MPa, 1820 MPa, and 1530 MPa for ligament size L_1 of 10 nm, 30 nm and 50 nm, respectively. Using the modified Roberts-Garboczi law for estimation of strength ($C = 0.5$, $m = 15/8$ also according to [15]) of the lower-level structure assuming a solid fraction $\varphi = 0.38$ and a percolation threshold $\varphi_{per} = 0.16$ results in 106 MPa, 73 MPa and 61 MPa as effective strength for NPG with the corresponding ligament sizes. The same calculation for the unimodal sample with a solid fraction of approximately 0.2 and a ligament strength of 804 MPa, corresponding to a ligament size of 330 nm, results in a strength of 1.5 MPa. Applying the scaling law for the hierarchical samples a second time for the upper hierarchy level with $\varphi = 0.52$ results in 10.6 MPa, 7.3 MPa, and 6.1 MPa as strength estimations for our HNPG with lower ligament size of 10 nm, 30 nm, and 50 nm respectively. These estimated values differ considerably from our experimental results as presented in Table 2 by a factor of approximately 4. This is not too surprising, since the relative densities are estimated under assuming equal shrinking during dealloying and no shrinking during post-annealing, resulting in a considerable uncertainty. And in our micro-compression experiments, the strength is determined as flow stress at 10% strain. But these hypothetical strength values reproduce very nicely the measured ligament size effect. Nevertheless, to understand this material more structural parameters must be taken into account and discussed.

The above discussions bring attention to the need for further systematic investigation on the relationship of microstructure and mechanical properties in the low relative density region. Given the challenge of making low-density NPG by typically dealloying, we would like to advertise here again that our strategy for fabricating nanoporous gold with low relative density might open the door to studying mechanical behavior and scaling equation for nanoporous gold extended to low relative density regions, which are still unclear and unexplored.

4.1.2. Connectivity

The connectivity can be one of the major parameters to determine the mechanical properties of nanoporous materials since only the connected ligaments (load-bearing ligaments) can support the applied load but the others (dangling ligaments) cannot contribute [12,40,47]. So, the higher connectivity can lead to higher mechanical properties in nanoporous materials. In order to compare the connectivity for coarsened nanoporous gold samples, the scaled connectivity density has been used, $C_v(1/S_v)^3$, where C_v is a connectivity density that is the number of closed loops per unit reconstructed volume, S_v is the specific surface area indicating the surface area per unit volume of ligaments, and the inverse of S_v, $1/S_v$, is used as the characteristic length scale. A good description and application of this concept on nanoporous gold can be found in [47–50]. Fig. 10 shows the scaled connectivity density $C_v(1/S_v)^3$ for HNPG with 30 nm, 50 nm, and NPG as determined by the FIB reconstructions. The scaled C_v are 0.00380 (±0.00020), 0.00351 (±0.00032), and 0.00036 (±0.00018) for HNPG with 30 nm, 50 nm, and NPG, respectively, as also listed in Table 3. This indicates that HNPG samples have around 10 times higher connectivity than that of NPG in terms of scaled C_v even though they maintain a similar relative density. Hence, the significant difference in connectivity can be considered as one of the major factors causing the remarkably enhanced mechanical properties in HNPG samples as compared to NPG.

The primary reason for such a huge difference of the connectivity in HNPG and NPG would be attributed to the amount of solid fraction at the structure during ligament coarsening. The studies on the topological evolution in nanoporous gold have suggested that the connectivity has evolved depending on its initial relative density [41,51]: above 30% relative density, the structure tends to maintain its connectivity during coarsening, whereas below 30%, the connectivity decreases. For HNPG, it would be reasonable to expect that the topological evolution throughout each of the two steps of thermal coarsening preserves a similar state as the initial state before coarsening, with only a minor decrease in connectivity if any. Solid fractions at both the upper- and

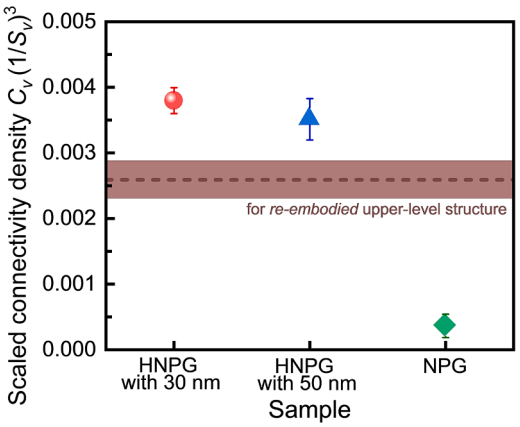

Fig. 10. Scaled connectivity density for HNPG with 30 nm, 50 nm, and NPG. Brown short-dash line is for the scaled connectivity density of upper-level structure in HNPG with the deviation marked by brown solid area, calculated from re-embodied upper-level structure. Average values are taken from at least 5 tests of each sample, with standard deviations represented by error bars.

Table 3
Structural values of HNPG with 30 nm, 50 nm, NPG, and re-embodied upper-level structure of HNPG: specific surface area, connectivity density, and scaled connectivity density, calculated from 3D reconstruction data.

	HNPG with 30 nm	HNPG with 50 nm	NPG	*Re*-embodied upper-level structure
Specific surface area, S_v [nm^{-1}]	0.0524 (±0.0011)	0.0515 (±0.0022)	0.0101 (±0.0007)	0.0111 (±0.0003)
Connectivity density, C_v [μm^{-3}]	546.6 (±51.1)	478.7 (±50.2)	0.4 (±0.1)	3.6 (±0.5)
Scaled connectivity density, $C_v(1/S_v)^3$	0.00380 (±0.00020)	0.00351 (±0.00032)	0.00036 (±0.00018)	0.00259 (±0.00029)

lower-level structure stayed above 30% throughout both coarsening processes: (1) during the first coarsening step to coarsen the structure of nanoporous $Ag_{70}Au_{30}$ alloy for defining the upper-level ligament size, it maintained around 52% solid fraction, and (2) during the second coarsening for lower-level ligaments, the solid fraction of lower-level structure retained around 38%. This step-by-step coarsening process for forming HNPG would help to prevent the loss of connectivity. Meanwhile, for NPG, during thermal coarsening to transition to the unimodal structure from the hierarchical structure, the collapse and rearrangement of ligaments would simultaneously occur throughout the entire hierarchical structures, both in the upper- and lower- levels. This indicates that the solid fraction of the structure that underwent thermal coarsening was around 20%, which corresponds to the overall relative density of the sample. This results in a significant loss of connectivity during the change from HNPG to NPG, in agreement with the low total relative density of the network structures. But still this loss seems less tremendous than the one happening in a typical one-step annealing procedure, as done in [11], see comparison in Fig. 9.

4.2. Plastic behavior

The strain hardening rate θ, from the $d\sigma/d\varepsilon$, where σ and ε are engineering stress and strain respectively, was determined as around 0.20–0.25 for HNPG with 10 nm, 30 nm, and 50 nm, and around 0.58 for NPG, irrespective of the environmental conditions. It is important to note that the value of θ from true stresses and strains would be lower than θ calculated from engineering stresses and strains. However, determining θ from the true stresses and strains would be challenging due to the non-existent volume conservation caused by the pore collapse and densification during plastic deformation.

The calculated θ indicates that NPG exhibits a typical strain hardening behavior during plastic deformation, similar to previous results of mechanical behavior in compressive tests for coarsened nanoporous gold [11,52-55]. HNPG, on the other hand, shows a diminished strain hardening in the plastic regime. Commonly, the strain-hardening phenomenon in nanoporous gold has been discussed in terms of the early contact of ligaments before reaching the densification regime due to the irregular structure and high relative density (20–42%) [11,52-55], unlike the sequential plastic collapse of structures and pores in cellular materials with a regular structure and low relative density (<10%) [56]. However, the concept of the early contact of structures cannot be a primary reason for the difference of strain hardening behavior between HNPG and NPG in this study. As presented in Fig. 6, in HNPG, the collapse of the structure favorably occurred at the upper-level structure, whereas the entire structure deformed in NPG. This implies that HNPG would have the higher probability for early contact as compared to NPG since it has the higher solid fraction that dominantly contributes to the plastic deformation: 52% solid fraction at upper-level structure in HNPG, but 20% solid fraction for entire structure in NPG.

4.2.1. Ligament-size distribution

The ligament-size distribution by the irregular nanoporous structure could cause a stochastically-sequential plastic deformation of ligaments: the first yielding initiates at the weakest ligament, e.g. geometrically the smallest-sized ligament, followed by subsequent yielding at the second, third, fourth weakest ligaments and so on. Thus, it implies that the required stress for further deformation will continue to increase in order to deform stochastically stronger (geometrically-larger) ligaments as long as they have a distribution of ligament sizes.

Fig. 11 presents the representative distribution of local thickness D scaled by the mean thickness $<D>$ and integrated area to 1 for HNPG with 30 nm, 50 nm, and NPG, along with the size-distributed 2D images for representative HNPG and NPG samples obtained from the reconstructed data. HNPG exhibited a markedly narrower distribution than NPG. This indicates that HNPG could statistically retain a more uniform distribution of ligament sizes with values closely clustered around the mean ligament size, whereas NPG has a broader distribution of ligament sizes. The narrow ligament-size distribution in HNPG would diminish this kind of apparent strain hardening since the required stress to deform further ligaments would be geometrically not much different from that for already deformed ones. For NPG, in contrast, the required stress for the consecutive collapse of ligaments would gradually increase as the plastic deformation proceeds, owing to stochastically wide-gaps of required stress for deforming two geometrically adjacent ligaments.

It is noteworthy that when considering the self-similar size distributions in coarsened nanoporous gold [47–49], the underlying mechanism for the narrower ligament-size distribution in HNPG is still unclear. This result may draw attention to further detailed studies analyzing the morphological evolution in HNPG, such as interfacial shape distribution (ISD) and interfacial normal distributions (IND).

4.2.2. Influence of ligament size on dislocation activities

As plastic deformation continues, dislocations can be governed either by initial dislocation sources or by nucleated new dislocations. The latter could occur when certain conditions are reached: all dislocations have escaped through the surface, or the initial dislocation sources themselves are rare. NPG with 330 nm ligament size could be large enough to exhibit a bulk-like behavior, which implies that the initial dislocation sources could serve as the dominant dislocation mechanism. This would induce a strain hardening by classical dislocation pileups rather than a dislocation starvation scenario during the plastic deformation, in line with the observation of the more pronounced strain-hardening behavior with increasing ligament size [11]. For HNPG, rather than the biased behavior, there could be a competition between initial dislocation sources and dislocation nucleation at slip

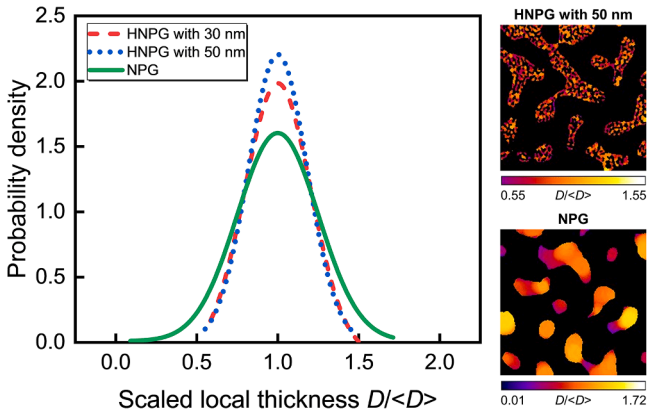

Fig. 11. Distribution of ligament size represented by scaled local thickness $D/<D>$, where D is local thickness and $\langle D \rangle$ is the mean thickness, for HNPG with 30 nm, 50 nm, and NPG, and the 2D images of thickness distribution for HNPG with 50 nm and NPG.

and/or surface steps for plasticity, contributing to the diminished strain hardening behavior. It is important to note that, although it is stochastically reasonable that ligaments of 10 nm to 50 nm are small enough to reach a dislocation-free condition that leads to dislocation nucleation governed plasticity, the characteristics of nanoporous gold could prompt a bulk-like behavior and suppress the dislocation escape in that (1) initial dislocations could inevitably exist in nanoporous gold induced by a volume contraction and/or surface-induced stresses [53,57], and (2) the dislocation movement could be impeded by the stress distribution by bending and/or shear of ligaments that is a dominant deformation mode in compression of nanoporous gold [11,58-61]. In addition, the absence of distinct strain-burst phenomena in the stress-strain curves implies that a full dislocation starvation did not occur in our results.

4.3. Electrochemically tunable flow stress

As presented in Figs. 4(e)–(h) and 5(b), the increase of flow stress induced by OH^- adsorption was distinctive in HNPG but negligible in NPG irrespective of compressive testing under the constant potential or potential jumps.

The suppressed role of capillary parameters, surface stress f and/or surface tension γ that tend to assist and ease the plastic deformation in the compressive loading, caused by the increased applied-potential and/or oxidized surface could contribute to the tunable flow stress [29,32]. However, both parameters did not seem to significantly contribute here since the compressive strength is clearly greater in HNPG samples even though f and γ should have higher impact on the stress due to the much smaller ligament size and higher surface-to-volume ratio as presented in Table 3 [29,62-64]. Obviously, the main causes for the difference in mechanical properties between HNPG and NPG are the connectivity and size effects on dislocation activities, and it would be difficult to uncouple the effect of them and the capillary parameters on the mechanical properties. Nevertheless, previous studies support that the capillary parameters might not be the primary contributors to the compressive flow stress in nanoporous gold, making only minor contribution if any: the stress variation by imposing the potential has not linearly scaled with the ligament size [31], and the compressive strengths have increased with decreasing ligament size [8,9,11,26].

Fig. 12 shows the stress variation ($\Delta\sigma/\sigma_0$) as a function of L_1 for HNPG and of L for NPG in addition to literature work on NPG reported so far [30–33]. It clearly indicates that the flow stress variations increase with decreasing ligament size, which is in accordance with the notion that the stress variation depends on the dominant dislocation mechanism [31]. It could be considered as a bulk-like behavior in NPG, and interaction of stochastic dislocations and surface nucleation of dislocations in HNPG, as the dominant dislocation mechanisms. Hence, HNPG, which could exhibit a more surface-sensitive behavior to the surface state, shows the more pronounced variation of flow stress by the monolayer oxide surface.

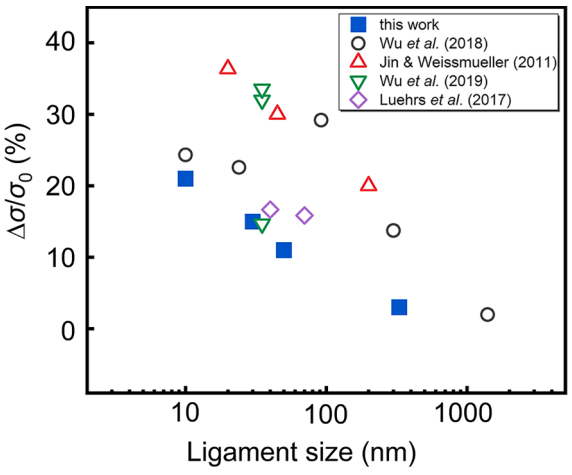

Fig. 12. Stress variation ($\Delta\sigma/\sigma_0$) versus ligament size of NPG or lower-level ligament size of HNPG.

Furthermore, as described above, the unnoticeable change of the strain hardening at the condition of 1.4 V compared to that of dry and −0.2 V may imply that the stresses in the ligaments during deformation are already so high that the monolayer oxide surface might not induce further strengthening by dislocation pinning at the surface regardless of whether it is HNPG or NPG.

4.4. Characteristic of hierarchical nanoporous gold

4.4.1. Governing structure-level contributing plastic deformation

By using the re-embodied upper-level structure as shown in Fig. 8(b), the scaled connectivity density for the upper-level structure was calculated as presented in Fig. 10 and Table 3, indicating that the scaled C_v for the upper-level structure is around 1.2 to 2.2 times smaller than that for total HNPG samples, but much higher than that for NPG. That is, even without consideration of size-effects, the upper-level structure in HNPG will primarily contribute to carrying the plastic deformation, aligning with the predominant structure-collapse at upper-level structure as manifested in Fig. 6 despite the fact that the relative density of the upper-level structure even is slightly higher than that of the lower-level structure. This may provide a further investigation into how the mechanical behavior of hierarchical nanoporous gold varies depending on the connectivity at upper-level structure and depending on the ratio of relative density at the upper- and lower-level structure while keeping the same overall relative density.

4.4.2. Lower-level ligament-size effect

In addition to the size effect on the dislocation sources mentioned in Section 4.1, the connectivity loss indiced by the insufficient ratio of the sizes between the upper- and lower-level ligaments (L_2/L_1) could be another reason for the decreasing flow stress with increasing L_1. Recently, Wu et al. [65] suggested a critical value of 20 for the ratio of pillar diameter (D) to ligament size (L) to exhibit comparable mechanical properties regardless of the ratio. Otherwise, the strength of the ligament network would decrease due to a non-negligeable influence of network parts which cannot contribute to mechanical stability due to the geometrical cuts by the surface. When considering L_2 of 320 nm and L_1 of 10 nm, 30 nm, and 50 nm for HNPG samples, $\alpha = L_2/L_1$ can be considered as 32, 11, and 6 for HNPG with 10 nm, 30 nm, and 50 nm, respectively. So, the trend of decreasing the ratio L_2/L_1 below $\alpha = 20$ with increasing L_1 could lead to a loss of connectivity, contributing to the ligament-size dependent flow stress at the lower-level structure.

The ligament-size effect on the dislocation behavior also increases the flow stress and stress variation ($\Delta\sigma/\sigma_0$). As described above, as the ligament size decreases, there will be fewer initial dislocations and the dislocation movement is strongly influenced by the surface state, causing a more surface-sensitive behavior. These trends lead to a strongly L_1 dependent flow stress and stress variation. Interestingly, it also causes a pronounced slope for the ligament-size dependent flow stress at 1.4 V (OS) condition compared to that in the condition of dry or −0.2 V (CS) due to the higher stress variation in the smaller L_1, as shown in Fig. 7(a). The size effect itself seems to have a dependence on the surface state.

In addition, as presented in Fig. 7(b), $\Delta\sigma/\sigma_0$ was similar for the strain near 15% and 25%, indicating that the stress variation is independent of the applied strain in this study. This could be attributed to the insignificant difference in strain-hardening behavior between the condition of 1.4 V and that of dry or −0.2 V. If the plastic behavior at 1.4 V exhibited a more pronounced strain-hardening rate, conjecturably due to the dislocation pileups caused by the surface pinning, the difference in the flow stress between at 1.4 V and −0.2 V (or dry) would also become larger as the strain increases, which consequently would lead to a larger

stress variation with increasing strain. The lack of these effects also implies that the changes in network structure during the deformation do not seem to have a significant influence on the dislocation size effect.

5. Conclusion

We investigated the mechanical behavior of hierarchical nanoporous gold by directly comparing it with unimodal nanoporous gold in an electrochemical environment. Despite both HNPG and NPG had a comparable relative density of 20%, the compressive strength in HNPG was much greater than that of NPG in all environmental conditions, and HNPG exhibited a distinct enhancement of the flow stress induced by the monolayer surface oxide at the applied potential of 1.4 V, while NPG showed an insensitive behavior to the change of surface state. In terms of the effect of lower-level ligament-size L_1 in HNPG, the flow stress increased with decreasing L_1 ranging from 10 nm to 50 nm, indicating a clear ligament-size effect, and the relative stress variation ($\Delta\sigma/\sigma_0$) also exhibited L_1-dependent behavior, a higher $\Delta\sigma/\sigma_0$ with smaller L_1, with comparable magnitude of $\Delta\sigma/\sigma_0$ regardless of applied strain.

One cause for the greater compressive strength in HNPG could be attributed to its higher connectivity, driving from the lower probability of losing the connectivity during the formation of structure through two separated coarsening steps while NPG revealed a significant loss of connectivity owing to its low relative density that underwent thermal coarsening. In addition, the different sizes that act as characteristic size in HNPG and NPG have a strong influence on the dislocation activities. HNPG exhibited a lower probability of dislocation accommodation, and the competitive nature between surface nucleation of dislocations (which dominates in the case of HNPG) and multiplication and gliding of initial dislocations (which dominates in the case of NPG) during deformation, resulting in a totally different mechanical behavior of these materials. For HNPG, this leads to a L_1-dependent flow stress and stress variation ($\Delta\sigma/\sigma_0$) as well as the pronounced stress variation by surface oxidation. On the other hand, the bulk-like behavior in NPG results in a low flow stress with strain hardening and negligible stress variation.

This study may raise further studies to understand underlying mechanisms of hierarchical nanoporous gold including morphological evolution, hierarchical-structural effects with uncoupled connectivity's effect, and the effect of the ratio of relative density between the upper- and lower-level structure, as well as exploring the connectivity of as-dealloyed HNPG with 3D reconstruction by reducing the difference in size between upper- and lower-level structures.

CRediT authorship contribution statement

Hansol Jeon: Conceptualization, Data curation, Formal analysis, Investigation, Methodology, Validation, Visualization, Writing – original draft, Writing – review & editing. **Jürgen Markmann:** Conceptualization, Data curation, Formal analysis, Funding acquisition, Investigation, Methodology, Project administration, Resources, Supervision, Writing – original draft, Writing – review & editing. **Shan Shi:** Conceptualization, Data curation, Formal analysis, Investigation, Methodology, Resources, Supervision, Writing – original draft, Writing – review & editing.

Declaration of competing interest

The authors declare that they have no known competing financial interests or personal relationships that could have appeared to influence the work reported in this paper.

Acknowledgments

This work was supported by the Deutsche Forschungsgemeinschaft (DFG, German Research Foundation) – project number 192346071 – SFB 986 "Tailor-Made Multi-Scale Materials Systems: M3".

References

[1] J. Biener, A. Wittstock, L.A. Zepeda-Ruiz, M.M. Biener, V. Zielasek, D. Kramer, R. N. Viswanath, J. Weissmüller, M. Baumer, A.V. Hamza, Surface-chemistry-driven actuation in nanoporous gold, Nat. Mater. 8 (1) (2009) 47–51.
[2] A. Wittstock, V. Zielasek, J. Biener, C.M. Friend, M. Bäumer, Nanoporous gold catalysts for selective gas-phase oxidative coupling of methanol at low temperature, Science (1979) 327 (5963) (2010) 319–322.
[3] C.A. Volkert, E.T. Lilleodden, D. Kramer, J. Weissmüller, Approaching the theoretical strength in nanoporous Au, Appl. Phys. Lett. 89 (6) (2006) 061920.
[4] J. Weissmüller, K. Sieradzki, Dealloyed nanoporous materials with interface-controlled behavior, Mrs. Bull 43 (1) (2018) 9–14.
[5] H.J. Jin, J. Weissmüller, D. Farkas, Mechanical response of nanoporous metals: a story of size, surface stress, and severed struts, Mrs. Bull 43 (1) (2018) 35–42.
[6] Y. Ding, Y.J. Kim, J. Erlebacher, Nanoporous gold leaf: "Ancient technology"/ advanced material, Adv. Mater. 16 (21) (2004) 1897–1900.
[7] F. Kertis, J. Snyder, L. Govada, S. Khurshid, N. Chayen, J. Erlebacher, Structure/ processing relationships in the fabrication of nanoporous gold, Jom-Us 62 (6) (2010) 50–56.
[8] J. Biener, A.M. Hodge, J.R. Hayes, C.A. Volkert, L.A. Zepeda-Ruiz, A.V. Hamza, F. F. Abraham, Size effects on the mechanical behavior of nanoporous Au, Nano Lett. 6 (10) (2006) 2379–2382.
[9] A.M. Hodge, J. Biener, J.R. Hayes, P.M. Bythrow, C.A. Volkert, A.V. Hamza, Scaling equation for yield strength of nanoporous open-cell foams, Acta Mater. 55 (4) (2007) 1343–1349.
[10] N.J. Briot, T.J. Balk, Developing scaling relations for the yield strength of nanoporous gold, Philos. Mag. 95 (27) (2015) 2955–2973.
[11] H. Jeon, S. Lee, J.Y. Kim, Tension-compression asymmetry in plasticity of nanoporous gold, Acta Mater. 199 (2020) 340–351.
[12] B. Zandersons, L. Luhrs, Y. Li, J. Weissmüller, On factors defining the mechanical behavior of nanoporous gold, Acta Mater. 215 (2021) 116979.
[13] E.J. Gwak, J.Y. Kim, Weakened flexural strength of nanocrystalline nanoporous gold by grain refinement, Nano Lett. 16 (4) (2016) 2497–2502.
[14] E.J. Gwak, H. Jeon, E.J. Song, N.R. Kang, J.Y. Kim, Twinned nanoporous gold with enhanced tensile strength, Acta Mater. 155 (2018) 253–261.
[15] S. Shi, Y. Li, B.N. Ngo-Dinh, J. Markmann, J. Weissmüller, Scaling behavior of stiffness and strength of hierarchical network nanomaterials, Science (1979) 371 (6533) (2021) 1026–1033.
[16] Z. Qi, J. Weissmüller, Hierarchical nested-network nanostructure by dealloying, ACS Nano 7 (7) (2013) 5948–5954.
[17] L. Riedel, J. Markmann, J. Weissmüller, S. Shi, Tailoring hierarchical nanoporous gold on dual length scales, Phys. Rev. Mater. 7 (11) (2023) 116001.
[18] Z. Qi, U. Vainio, A. Kornowski, M. Ritter, H. Weller, H.J. Jin, J. Weissmüller, Porous gold with a nested-network architecture and ultrafine structure, Adv. Funct. Mater. 25 (17) (2015) 2530–2536.
[19] Y. Ding, J. Erlebacher, Nanoporous metals with controlled multimodal pore size distribution, J. Am. Chem. Soc. 125 (26) (2003) 7772–7773.
[20] X.W. Guo, J.H. Han, P. Liu, L.Y. Chen, Y. Ito, Z.L. Jian, T.N. Jin, A. Hirata, F.J. Li, T. Fujita, N. Asao, H.S. Zhou, M.W. Chen, Hierarchical nanoporosity enhanced reversible capacity of bicontinuous nanoporous metal based LiO_2 battery, Sci. Rep. 6 (2016) 33466.
[21] F. Liu, X.L. Ye, H.J. Jin, Anomalous low strain induced by surface charge in nanoporous gold with low relative density, Phys. Chem. Chem. Phys. 19 (29) (2017) 19217–19224.
[22] J.R. Greer, W.C. Oliver, W.D. Nix, Size dependence of mechanical properties of gold at the micron scale in the absence of strain gradients, Acta Mater. 53 (6) (2005) 1821–1830.
[23] J.R. Greer, J.T.M. De Hosson, Plasticity in small-sized metallic systems: intrinsic versus extrinsic size effect, Prog. Mater. Sci. 56 (6) (2011) 654–724.
[24] C.A. Volkert, E.T. Lilleodden, Size effects in the deformation of sub-micron Au columns, Philos. Mag. 86 (33–35) (2006) 5567–5579.
[25] D. Mordehai, S.W. Lee, B. Backes, D.J. Srolovitz, W.D. Nix, E. Rabkin, Size effect in compression of single-crystal gold microparticles, Acta Mater. 59 (13) (2011) 5202–5215.
[26] Y.C. Kim, E.J. Gwak, S.M. Ahn, J.I. Jang, H.N. Han, J.Y. Kim, Indentation size effect in nanoporous gold, Acta Mater. 138 (2017) 52–60.
[27] Y.Y. Zhang, H. Xie, L.Z. Liu, H.J. Jin, Surface triple junctions govern the strength of a nanoscale solid, Phys. Rev. Lett. 126 (23) (2021) 235501.
[28] H. Jeon, J.H. Woo, E. Song, J.Y. Kim, Ligament size effect in creep of nanoporous gold, Int. J. Plastic. 150 (2022) 103192.
[29] N. Mameka, J. Markmann, J. Weissmüller, On the impact of capillarity for strength at the nanoscale, Nat. Commun. 8 (2017) 1976.
[30] H.J. Jin, J. Weissmüller, A material with electrically tunable strength and flow stress, Science (1979) 332 (6034) (2011) 1179–1182.
[31] P. Wu, X.L. Ye, L.Z. Liu, H.J. Jin, Monolayer oxide enhanced flow stress in nanoporous gold: the size dependence, Mater. Res. Lett. 6 (9) (2018) 508–514.
[32] L. Lührs, B. Zandersons, N. Huber, J. Weissmüller, Plastic Poisson's ratio of nanoporous metals: a macroscopic signature of tension-compression asymmetry at the nanoscale, Nano Lett. 17 (10) (2017) 6258–6266.
[33] Y.J. Wu, J. Markmann, E.T. Lilleodden, Electro-chemo-mechanical coupling of nanoporous gold at the microscale, Appl. Phys. Lett. 115 (25) (2019) 251602.
[34] J. Schindelin, I. Arganda-Carreras, E. Frise, V. Kaynig, M. Longair, T. Pietzsch, S. Preibisch, C. Rueden, S. Saalfeld, B. Schmid, J.Y. Tinevez, D.J. White, V. Hartenstein, K. Eliceiri, P. Tomancak, A. Cardona, Fiji: an open-source platform for biological-image analysis, Nat. Method. 9 (7) (2012) 676–682.

[35] M. Doube, M.M. Klosowski, I. Arganda-Carreras, F.P. Cordelières, R.P. Dougherty, J.S. Jackson, B. Schmid, J.R. Hutchinson, S.J. Shefelbine, BoneJ Free and extensible bone image analysis in ImageJ, Bone 47 (6) (2010) 1076–1079.
[36] L.H. Qian, M.W. Chen, Ultrafine nanoporous gold by low-temperature dealloying and kinetics of nanopore formation, Appl. Phys. Lett. 91 (8) (2007) 083105.
[37] Y.C.K. Chen-Wiegart, S. Wang, Y.S. Chu, W.J. Liu, I. McNulty, P.W. Voorhees, D. C. Dunand, Structural evolution of nanoporous gold during thermal coarsening, Acta Mater. 60 (12) (2012) 4972–4981.
[38] G. Pia, A. Cincotti, F. Delogu, Thermally and catalytically induced coarsening of nanoporous Au, Mater. Lett. 183 (2016) 114–116.
[39] G. Son, Y. Son, H. Jeon, J.Y. Kim, S. Lee, A three-dimensional Monte Carlo model for coarsening kinetics of the bi-continuous system via surface diffusion and its application to nanoporous gold, Scripta Mater. 174 (2020) 33–38.
[40] L.Z. Liu, X.L. Ye, H.J. Jin, Interpreting anomalous low-strength and low-stiffness of nanoporous gold: quantification of network connectivity, Acta Mater. 118 (2016) 77–87.
[41] H. Xie, H. Guan, L.Z. Liu, H.J. Jin, A critical relative density and a break-and-reconnect model for annealing-induced densification in nanoporous gold, Acta Mater. 209 (2021) 116806.
[42] S.H. Oh, M. Legros, D. Kiener, G. Dehm, In situ observation of dislocation nucleation and escape in a submicrometre aluminium single crystal, Nat. Mater. 8 (2) (2009) 95–100.
[43] A.T. Jennings, C. Gross, F. Greer, Z.H. Aitken, S.W. Lee, C.R. Weinberger, J. R. Greer, Higher compressive strengths and the Bauschinger effect in conformally passivated copper nanopillars, Acta Mater. 60 (8) (2012) 3444–3455.
[44] S.W. Lee, A.T. Jennings, J.R. Greer, Emergence of enhanced strengths and Bauschinger effect in conformally passivated copper nanopillars as revealed by dislocation dynamics, Acta Mater. 61 (6) (2013) 1872–1885.
[45] S. Shao, N. Abdolrahim, D.F. Bahr, G. Lin, H.M. Zbib, Stochastic effects in plasticity in small volumes, Int. J. Plastic. 52 (2014) 117–132.
[46] I. Ryu, W. Cai, W.D. Nix, H.J. Gao, Stochastic behaviors in plastic deformation of face-centered cubic micropillars governed by surface nucleation and truncated source operation, Acta Mater. 95 (2015) 176–183.
[47] K.X. Hu, M. Ziehmer, K. Wang, E.T. Lilleodden, Nanoporous gold: 3D structural analyses of representative volumes and their implications on scaling relations of mechanical behaviour, Philos. Mag. 96 (32–34) (2016) 3322–3335.
[48] M. Ziehmer, K.X. Hu, K. Wang, E.T. Lilleodden, A principle curvatures analysis of the isothermal evolution of nanoporous gold: quantifying the characteristic length-scales, Acta Mater. 120 (2016) 24–31.
[49] H. Jeon, N.R. Kang, E.J. Gwak, J.I. Jang, H.N. Han, J.Y. Hwang, S. Lee, J.Y. Kim, Self-similarity in the structure of coarsened nanoporous gold, Scripta Mater. 137 (2017) 46–49.
[50] M. Ziehmer, E.T. Lilleodden, The isothermal evolution of nanoporous gold from the ring perspective - an application of graph theory, Acta Mater. 199 (2020) 669–679.
[51] Y. Li, B.N.D. Ngo, J. Markmann, J. Weissmüller, Topology evolution during coarsening of nanoscale metal network structures, Phys. Rev. Mater. 3 (7) (2019) 076001.
[52] H.J. Jin, L. Kurmanaeva, J. Schmauch, H. Rösner, Y. Ivanisenko, J. Weissmuller, Deforming nanoporous metal: role of lattice coherency, Acta Mater. 57 (9) (2009) 2665–2672.
[53] B.N.D. Ngo, A. Stukowski, N. Mameka, J. Markmann, K. Albe, J. Weissmüller, Anomalous compliance and early yielding of nanoporous gold, Acta Mater. 93 (2015) 144–155.
[54] C.J. Ruestes, D. Farkas, A. Caro, E.M. Bringa, Hardening under compression in Au foams, Acta Mater. 108 (2016) 1–7.
[55] M. Burckert, N.J. Briot, T.J. Balk, Uniaxial compression testing of bulk nanoporous gold, Philos. Mag. 97 (15) (2017) 1157–1178.
[56] L.J. Gibson, M.F. Ashby, Cellular Solids: Structure and Properties, Cambridge Univ. Press., Cambridge, 1997.
[57] S. Parida, D. Kramer, C.A. Volkert, H. Rosner, J. Erlebacher, J. Weissmüller, Volume change during the formation of nanoporous gold by dealloying, Phys. Rev. Lett. 97 (3) (2006) 035504.
[58] N.A. Fleck, G.M. Muller, M.F. Ashby, J.W. Hutchinson, Strain gradient plasticity - theory and experiment, Acta Metall. Mater. 42 (2) (1994) 475–487.
[59] C. Motz, T. Schoberl, R. Pippan, Mechanical properties of micro-sized copper bending beams machined by the focused ion beam technique, Acta Mater. 53 (15) (2005) 4269–4279.
[60] D. Kiener, C. Motz, T. Schoberl, M. Jenko, G. Dehm, Determination of mechanical properties of copper at the micron scale, Adv. Eng. Mater. 8 (11) (2006) 1119–1125.
[61] C. Motz, D. Weygand, J. Senger, P. Gumbsch, Micro-bending tests: a comparison between three-dimensional discrete dislocation dynamics simulations and experiments, Acta Mater. 56 (9) (2008) 1942–1955.
[62] D. Kramer, J. Weissmüller, A note on surface stress and surface tension and their interrelation via Shuttleworth's equation and the Lippmann equation, Surf. Sci. 601 (14) (2007) 3042–3051.
[63] D.A. Crowson, D. Farkas, S.G. Corcoran, Mechanical stability of nanoporous metals with small ligament sizes, Scripta Mater. 61 (5) (2009) 497–499.
[64] N. Beets, D. Farkas, S. Corcoran, Deformation mechanisms and scaling relations in the mechanical response of nano-porous Au, Acta Mater. 165 (2019) 626–637.
[65] Y. Wu, J. Markmann, E.T. Lilleodden, On the consequences of intrinsic and extrinsic size effects on the mechanical response of nanoporous Au, Mater. Des. 232 (2023).